The Egyptian Journal of Radiology and Nuclear Medicine (2016) 47, 127–139

Egyptian Society of Radiology and Nuclear Medicine

The Egyptian Journal of Radiology and Nuclear Medicine

www.elsevier.com/locate/ejrnm
www.sciencedirect.com

ORIGINAL ARTICLE

Accuracy assessment of combined diffusion weighed and dynamic gadolinium MR sequences in characterization of salivary gland tumors

Lamya Eissa [a,*], Shadia Abou Seif [a], Salah El Desooky [a], Mohamed Eid [a], Tarek Koraitim [b]

[a] *Radiology Department, Alexandria University, Egypt*
[b] *Head and Neck Surgery Department, Alexandria University, Egypt*

Received 28 February 2015; accepted 23 November 2015
Available online 6 January 2016

KEYWORDS

Diffusion;
Dynamic MRI;
Parotid neoplasms

Abstract *Background:* The salivary glandular tumors are challenging as regards preoperative diagnosis and MRI with the use of DWI and DCE are evaluated in accuracy for characterization of salivary masses.
Methods: The study included 53 patients who underwent MRI-DWI and DCE and diagnosis was made by diagnostic scheme of ADC-values and four types of DCE curves.
Results: Pleomorphic adenomas had the highest of all ADC values on DWI ($\geqslant 1.4 \times 10^{-3}$ cm^2/s), and Warthin tumors had low values ($0.6–0.8 \times 10^{-3}$ cm^2/s), while malignant tumors had intermediate values ($0.8–1.2 \times 10^{-3}$ cm^2/s). Type A curve predominated the pleomorphic adenomas, type B curve predominated Warthin, and other lymphoid lesions as lymphoma. Type C curve predominated malignant lesions. Statistical analysis showed combination intermediate ADC (in range of 0.8 to $< 1.4 \times 10^{-3}$ cm^2/s) and type C as useful test of malignancy with high accuracy of 90.5%.
Conclusion: DWI and dynamic enhancement curves with combined interpretation of both techniques and in view of the concluded values can provide valuable data in characterization of salivary glandular tumors.

1. Introduction

Salivary gland tumors account for only 3% of all tumors in the body and it is estimated that about 1% of all head and neck malignant neoplasms arise in the salivary glands (1–3). However, the great variety of histological types makes them a major challenge for radiologists and clinicians. Fine needle aspiration cytology (FNAC) is not always conclusive; there is a selection bias and when the tumor is located in the deep lobe, FNAC cannot be performed in all cases. Therefore, preoperative imaging has a major role in surgical planning (2,3). Conventional MRI imaging of these lesions had shown some suggestive features; T2 bright signal and polylobulation have

* Corresponding author.
Peer review under responsibility of Egyptian Society of Radiology and Nuclear Medicine.

http://dx.doi.org/10.1016/j.ejrnm.2015.11.011

suggested pleomorphic adenoma, and T2 hypo-intensity and cystic changes favored Warthin, while diagnosis of malignant tumors may be suggested in case of high-grade lesions with infiltrative margins. However, conventional features alone cannot adequately characterize parotid lesions. The purpose of this work was to evaluate the potential use of dedicated MRI sequences of diffusion and dynamic curves in preoperative characterization of salivary glandular tumors.

2. Patients, materials and methods

2.1. Patient population

This study was conducted in accordance with the local ethics committee and included 53 patients, presented to our Radiology Department in a prospective study in the period from July 2013 to January 2015.

The patients had clinically palpable lesions of the major salivary glands suspected to be tumors and imaging was requested for the aim of diagnosis and local staging purpose.

The parotid lesions constituted the majority, contributing 45 out of the total 53 cases, with single case of submandibular, two cases of minor salivary glands (palate and floor of mouth) and 5 parotidectomies.

The study included 28 females and 25 males with age range from 20 to 75 years (pediatric age <18 have been excluded).

Following DW-MRI, 47 masses were surgically biopsied or resected (36 parotidectomies, 8 enucleation, excision of palatal, floor of sublingual and submandibular lesions), 3 were cytologically analyzed via US-FNAC, and 2 had nodes assessed by nodal FNAC or excision. CT chest in one case of parotid deposit showed primary bronchogenic carcinoma.

2.2. MRI technique and methods

The MRI examination studies were made on closed 1.5 Tesla magnets (Siemens; Avanto, Germany).

Dedicated multichannel head and neck coil has been used. Our Neck MRI exam included the following sequences: Axial T1 turbo spin echo (TSE) Without Fat suppression, Axial T2 Turbo-spin echo with fat suppression, and axial and Coronal T2 sequence without fat suppression.

- For routine sequences a slice thickness of 5 mm was used with inter-slice gap of 3 mm, and a 16×16 cm field of view (FOV), with 2 averages used. Spin echo T1 weighted images used (TR, 400 ms; TE, 10 ms; 256×256 matrix), turbo spin-echo T2 weighed (TR, 4400 ms; TE, 105 ms; 250×250 matrix).
- First diffusion images are taken before injection of contrast. These diffusion images use single shot spin echo planar imaging (SS-EPI) in axial plane, with fat suppression made by chemical shift selective fat suppression. Diffusion was obtained by "High" repetition time (TR) 1700 ms, "short" echo time (TE) 100 ms, "Coarse" matrix, 192×144; slice numbers, 30; slice thickness = 5 mm; interslice gap, 35%; FOV, 25 cm; averages, 5; acquisition time approximately 1 min 45 s. "Three b-factors " are obtained including 0, 500 and 1000 s/mm^2 in the axial plane.
- Following diffusion, dynamic MRI sequence was made by injection of Gadolinium Gadopentate Dimeglumine with a dose of 0.1 mmol/kg and at a rate of 2 ml/s using power injector followed by 20 ml saline flush. Sequential images were obtained through the lesion in axial plane and at different time intervals (at 30, 60, 90, 120, 150, 180, 240 and 300 s following injection). Following dynamic acquisition, conventional post contrast MRI images are acquired in the axial, sagittal and coronal planes.

2.3. Image analysis

2.3.1. Image analysis of diffusion images

A region of interest (ROI) was drawn on the tumor by two experienced head and neck radiologists (more than 8 years experience in Head and Neck Radiology). This ROI is drawn on solid portion of the tumor. It must be sufficient, at least 1/2 of the tumor cross-sectional area in given axial slice. Areas of hemorrhage or necrosis are avoided.

2.3.2. Post processing and image analysis for DCE-MRI

The time–intensity curves were generated on dedicated Siemens software after drawing the ROI on the lesion, which covers the solid enhancing portion of the lesion. Vessels, necrosis, calcifications and hemorrhages are avoided. Sufficient ROI must be obtained (at least 50% of cross-sectional area). Dynamic enhancement curves are described according to Yabuuchi et al. (4) in Fig. 1 and diagnosis is made according to scheme in Fig. 2.

2.4. Statistical analysis

Data were fed to the computer and analyzed using IBM SPSS software package version 20 (2). The distributions of quantitative variables (ADC-values) were tested for normality using Kolmogorov–Smirnov test. For abnormally distributed data Kruskal Wallis test was used to compare between different groups and Mann–Whitney Test was assessed for pair-wise comparisons. Receiver operating characteristic curve (ROC) was plotted to analyze a recommended cutoff, and the area under the ROC curve denotes the diagnostic performance of the test. Area more than 50% gives acceptable performance and area about 100% is the best performance for the test. Significance of the obtained results was judged at the 5% level (see Figs. 3–9).

3. Results

3.1. Patients demographics and general distribution of histopathological lesions

Age and sex demographics showed 28 females and 25 males with age range from 20 to 75 years. The parotid lesions constituted the majority, contributing 45 out of the total 53 cases, with single case of submandibular, two cases of minor salivary glands (palate and floor of mouth), and 5 parotidectomy cases (Table 1).

As expected benign lesions took the upper hand overall 41 out of 53 cases with benign pathology (constituting 77.4%) against 12 cases of malignant pathology (constituting 22.6%). Benign mixed tumor represented the most common tumor ($n = 21$) and represented 63% of benign lesions and

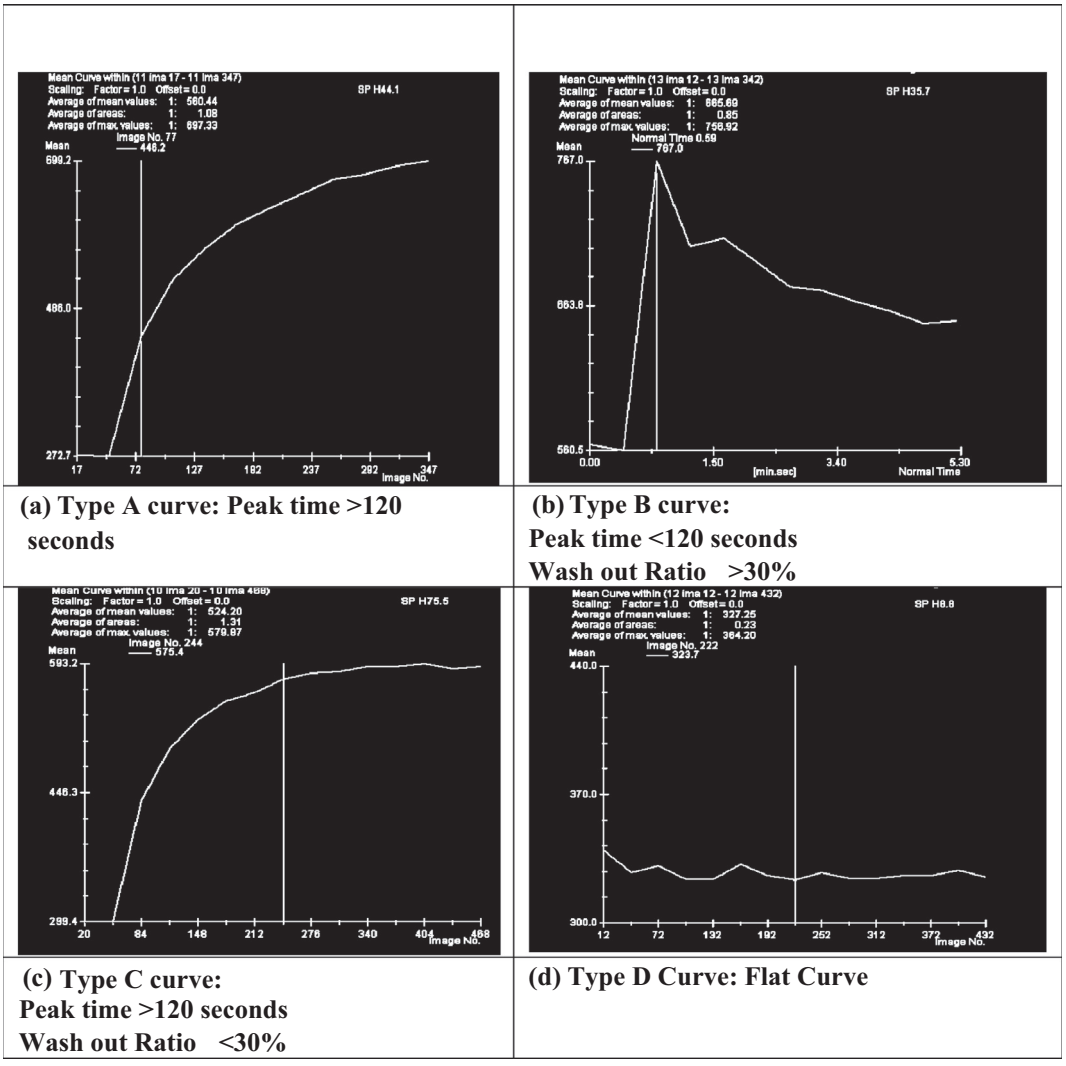

Fig. 1 Types of TIC curves. Yabuuchi et al. (3)

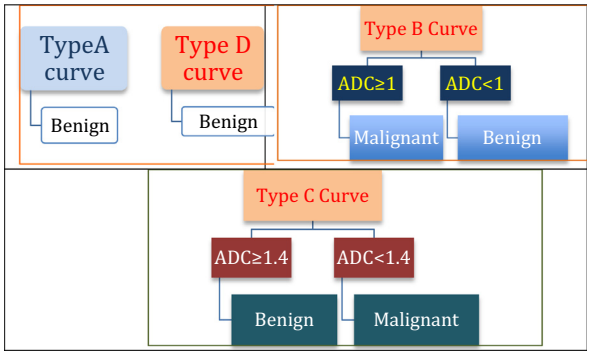

Fig. 2 Diagnostic scheme according to Yabuuchi et al. (3)

40% of all tumors. Warthin tumor (n = 11) was the second most common tumor and showed high percentage representing about 33% of benign tumors. Malignant tumors included (n = 12) including (n – 9 primary malignancy, n = 2 lymphomas, One HD and the other NHL and 1 = metastasis from bronchogenic carcinoma) primary malignancy distributed as follows: 3 with acinic cell carcinoma, 2 with mucoepidermoid carcinoma, 2 with SCC, single case of adenoid cystic carcinoma with extensive perineural spread along the facial and great auricular nerves. Non-tumoral lesions (n = 8) included one cyst, four lymph nodes, one lymphoepithelial lesion and two chronic abscesses. A single case of rare intraparotid schwannoma was included.

Pleomorphic adenomas showed higher ratio in females (17 females versus 4 males). In total, 21 cases of pleomorphic adenomas, 19 parotids, 1 submandibular and 1 palatal were found; among them, 3 were recurrent lesions, size ranging from 1 to 9 cm, and one case showed bilateral parotids. 19 cases had type A curves, and only two had type C curve. ADC-range ($1.4–2.2 \times 10^{-3}$ cm^2/s). Only 3 cases had iso to hyperintensity and others showed bright signal. All showed strong enhancement.

The study included 11 cases of Warthin tumor, age range was 47–72 years, size range (1.3–4 cm); the majority (9) are men and only two females. Three cases were bilateral, and 5 occurred in the tail. T2 signal was predominantly hypo or

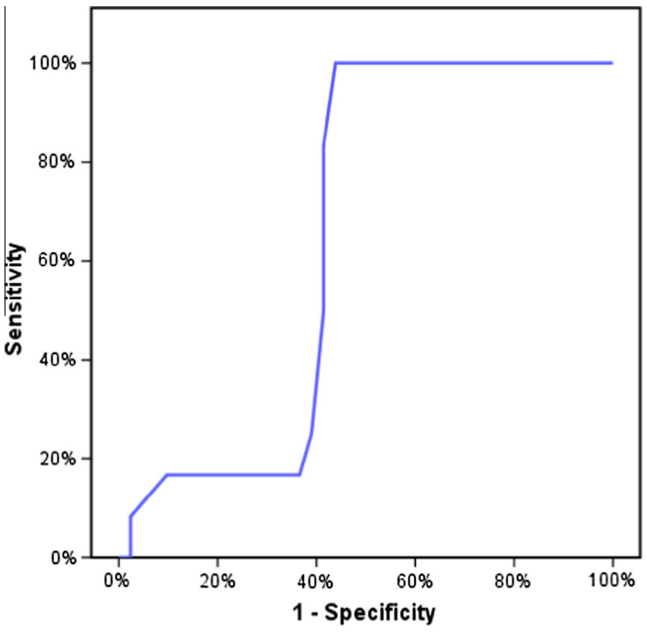

Fig. 3 ROC curve.

iso, and never hyperintense. All had type B curve. They had ADC-values in range of 0.6–0.8 $\times$ 10^{-3} cm^2/s.

Malignant tumors showed slightly higher male ratio, 7 out of 9 primary malignancies showed type C curve and they showed ADC-range of 0.8–1.2 $\times$ 10^{-3} cm^2/s. Of the remaining two malignant cases, one case had type A curve (Carcinoma ex-pleomorphic adenoma) and one had type B curve.

3.2. Results of DWI: This included descriptive and analytic analyses

3.2.1. Descriptive analysis of DWI data

Lesions were classified according to ADC values into Low, Intermediate and High ADC values (Table 2).

(I) Low ADC value <0.8: ($n = 15$) this group included all lymphoid lesions of the parotid glands: 10 Warthin (66.7%), the two Lymphoma cases (13.3%), single Benign Lympho-epithelial lesion (6.7%), two cases of Benign Lymph nodes (13.3%).

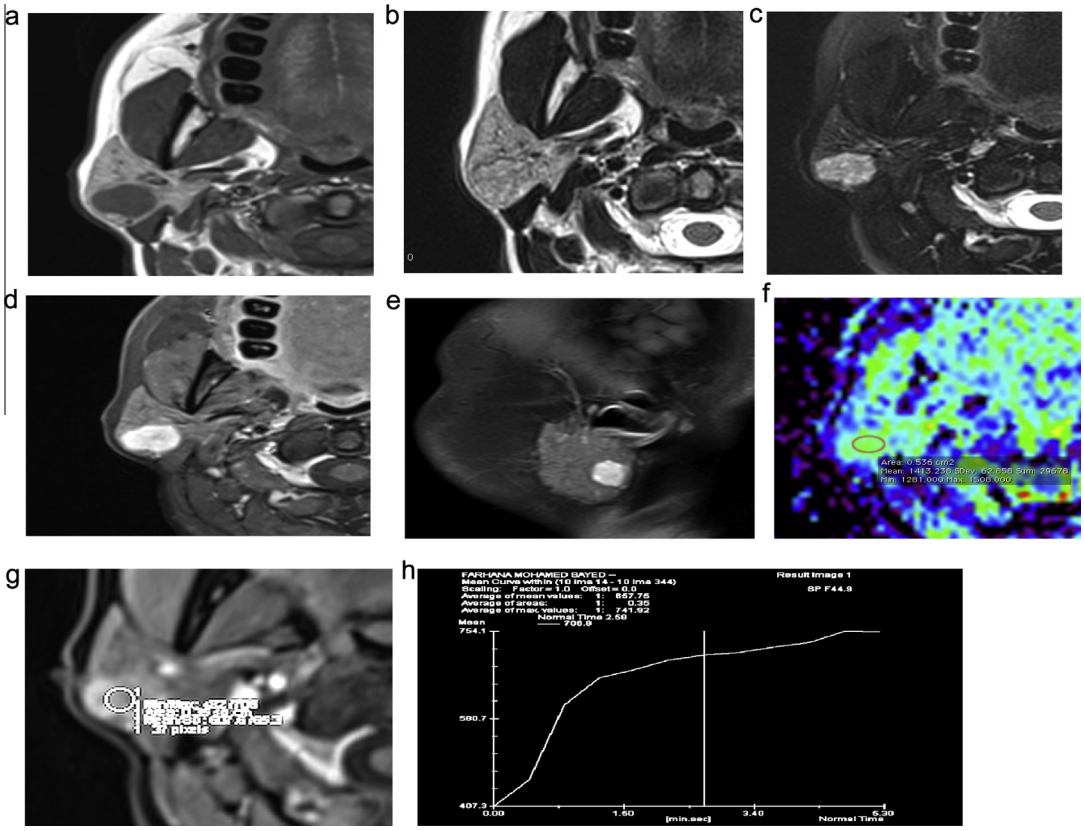

Fig. 4 Case 1: Pleomorphic adenoma. A 32 years old female presenting with right painless parotid mass. (a) Axial T1 shows homogenously hypo-intense lesion. (b and c) Axial T2 showed nearly iso-intense signal to slightly hyperintense becoming hyper to bright in axial STIR. (e and f) Axial and coronal post GAD images show strong homogenous contrast enhancement. (f) High ADC value of 1.4 $\times$ 10 is seen. (g and h) Show ROI placement in the lesion generating type A curve. *Conclusion:* Although slight hyperintensity is not typical of pleomorphic adenoma, combination of high >1.4 ADC, type A curve and STIR bright signal leads to conclusion of pleomorphic adenoma, suggested by FNA later and confirmed post superficial parotidectomy.

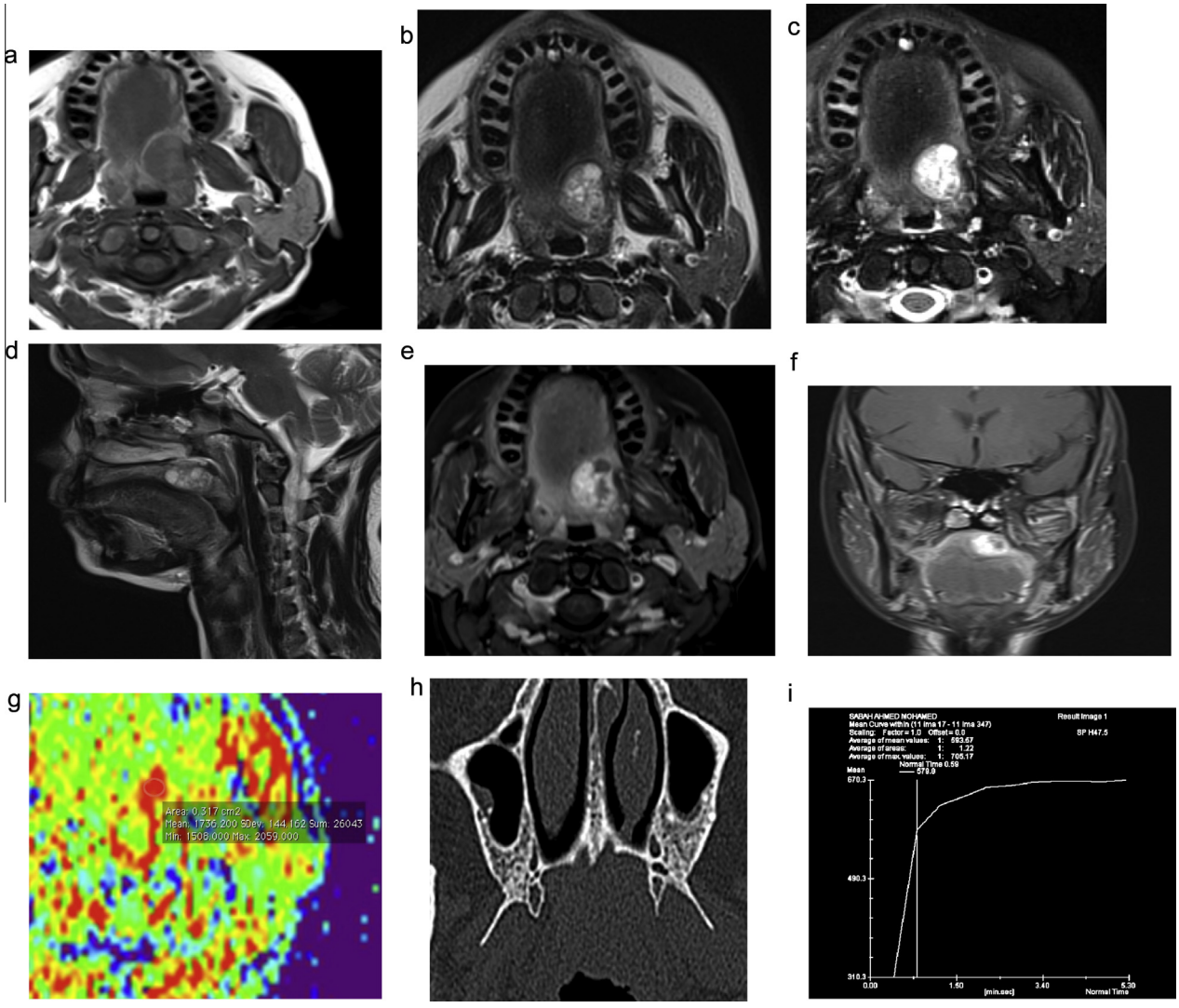

Fig. 5 Case 2: Pleomorphic adenoma. A 32 years old female presenting with oral mass and dysphagia. (a) Axial T1 WI shows smooth well-marginated lesion at the left side of the palate. (b) Axial T2WI shows bright signal and thin internal septa. (c) Axial STIR shows more bright signal. (d) Sagittal T2WI shows the lesion at the junction of hard and soft palates. (e and f) Axial and coronal T1 + GAD images showed strong enhancement with cystic changes. (g) Color scale ADC showed high ADC of 1.7×10^{-3} cm^2/s. (h) Non-contrast CT showed smooth scalloping of the hard palate. (i) Type A curve is displayed by the lesion. Imaging diagnosis suggested pleomorphic adenoma proven later by post surgical biopsy.

(II) Intermediate ADC value: (n = 12) 0.8 to <1.4: majority of this group (10 cases) are primary malignant lesions, and a single case of Benign lymph nodes and a single Warthin lesion.
(III) High ADC value: $\geqslant 1.4$ (n = 21): Only benign lesions occupied this group (Pleomorphic adenoma and the single case of cyst).

3.2.2. Statistical analysis of DWI data

A. Determination of cutoff value: This was made in order to determine a particular ADC value to be used as a cut-off value for differentiation between benign and malignant tumors. Analysis of the ROC curve yielded a cutoff point for the ADC value at 1.30 and 1.2 with 100% sensitivity, 56% specificity, 40% positive and 100% negative predictive values respectively.
B. Comparison between different pathological subtypes (Table 3) was made to compare between ADC values of different pathological groups to determine whether there is significant difference with calculation of p-value (see Table 4).
C. Determination of accuracy of certain ADC values in characterization of tumors (Table 5):
   a. High ADC value $\geqslant 1.4 \times 10^{-3}$ cm^2/s was tested a sign of benignity: This showed 100% sensitivity and moderate specificity of 56%, low PPV of 40%, high NPV of 10% and moderate accuracy of 66%.

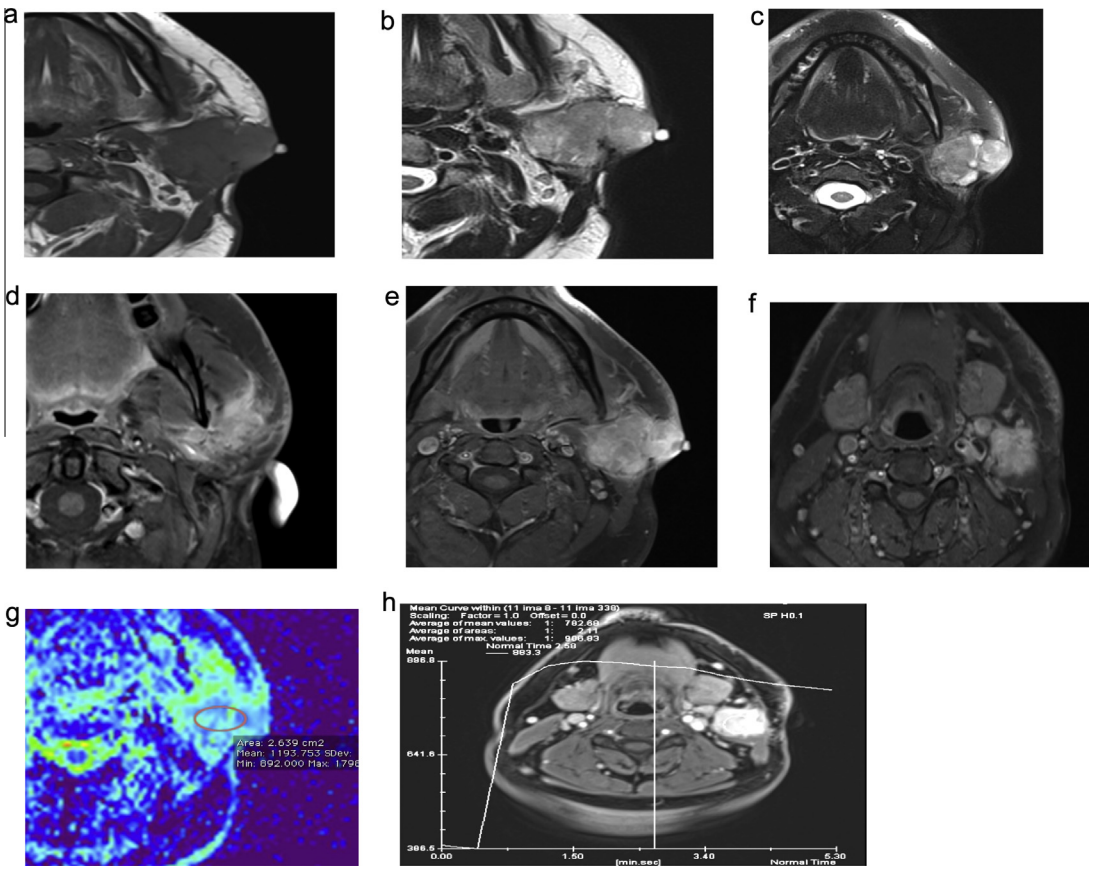

Fig. 6 Case 3: Malignancy on top of pleomorphic adenoma. A 34 years old male with known history of repeated surgeries (enucleation and superficial parotidectomy) for pleomorphic adenoma. Now the patient is presenting with rapidly enlarging mass at left parotidectomy bed with stretching of overlying skin. (a) Axial T1 shows lobulated and irregularly marginated lesion with extra-capsular growth. (b and c) Axial T2 and STIR images showed iso-intense heterogeneous signal. (d and e) Post GAD images showed moderate heterogeneous enhancement with infiltrative margins in direct contact with sternomastoid muscles. A rounded lymph node is seen in ipsilateral upper deep cervical group (Level IA). (g) ADC map showed intermediate value of 1.2×10^{-3} cm^2/s. (h) Post GAD generated curve is type C (Plateau curve). Conclusion is made of malignancy on top of pleomorphic adenoma. Later biopsy confirmed Carcinoma ex-pleomorphic.

b. Intermediate ADC (in range of 0.8 to $< 1.4 \times 10^{-3}$ cm^2/s) was tested as test of malignancy against other values outside the range; this showed a useful test of malignancy showing sensitivity of 83.3%, high specificity of 92.6%, low PPV of 76.9%, high NPV of 95% and moderate accuracy of 90.57%.

3.3. Analysis of DCE curve

3.3.1. Descriptive analysis

Four types of Dynamic Contrast Enhancement were generated from lesions (Table 6).

These are distributed among lesions as follows:

A. Type A-curve: this was generated by 19 benign mixed tumors, the single Schwanoma case, and one malignant case of Muco-epidermoid carcinoma (this developed on top of BMT)
B. Type B-curve: this was revealed from ALL eleven Warthin cases, 3 benign lymph nodes, the two cases of Lymphoma, the single case of BLEL, and a single malignant case of Acinic cell carcinoma.
C. Type C-curve: this was generated from 7 primary malignancies, two benign mixed tumors, one lymph node, and two chronic abscesses.
D. Type D-curve (Flat curve): this was found in one case only (benign cyst).

3.3.2. Statistical analysis of dynamic curves

A. Type A curve was tested a test of benignity against other types of curves: This showed 90% sensitivity and specificity of only 50%, low PPV of 33%, high NPV of 95% and accuracy of 58.8% (Table 7).
B. Type C curve was tested a test of Malignancy against other types of curves. This showed moderate 63% sensitivity and high specificity of 87.5%, PPV of 58%, high NPV of 89.7% and good accuracy of 82.3%.

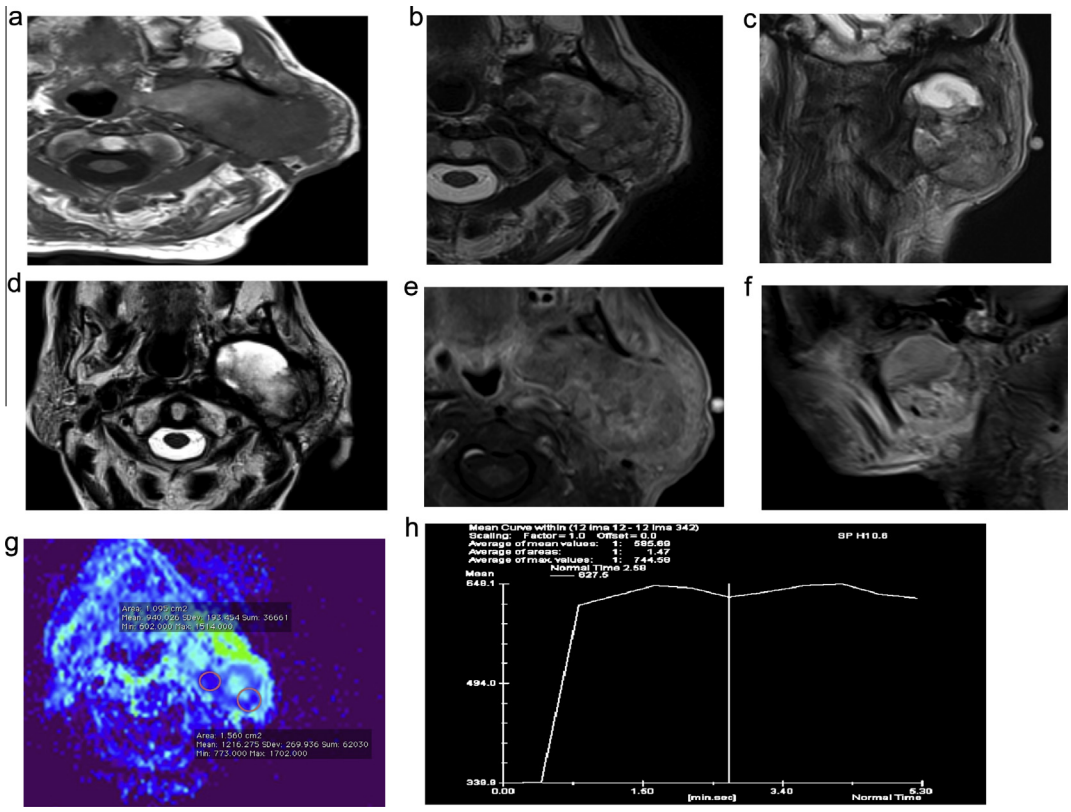

Fig. 7 Case 4: Mucoepidermoid carcinoma. A 76 years old female presenting with slowly growing parotid mass on the left side for average duration of 9 months. No pain and no facial nerve palsy. (a) Axial non-contrast T1 image shows heterogeneously hypo-intense mass seen in superficial lobe of left parotid and growing into deep lobe and parapharyngeal space. Focal area of extracapsular growth is seen (short block arrow). (b) Axial T2 image shows heterogeneous predominantly hypo-intense signal. (c and d) Coronal and axial T2 showed proximal cystic degeneration of the mass lesion. (e and f) Axial and sagittal pots contrast T1 images revealed markedly heterogeneous moderate solid enhancement of the mass. (g) Showed color scale ADC map revealing intermediate ADC of 1.2. (h) DCE type C curve, low wash out ratio (Plateau curve). *Conclusion* was made of malignant mass. Later surgical biopsy proved Mucoepidermoid carcinoma.

3.3.3. Analysis of combined ADC values and DCE curves

A. Combination of Type A curve and High ADC value $\geqslant 1.4 \times 10^{-3}$ cm^2/s was tested a test of benignity against others: This showed 100% sensitivity and specificity of only 48.3%, low PPV of 34%, high NPV of 100% and accuracy of 59.6% (Table 8).
B. Combination of Type C curve and Intermediate ADC values (0.8–1.4) $\times 10^{-3}$ cm^2/s was tested a test of malignancy against others: This showed 63% sensitivity and high specificity of 97.6%, high PPV of 87%, high NPV of 90% and high accuracy of 90%.

4. Discussion

The salivary glands are rare tumors and represent the most heterogeneous group of tumors in the whole body regarding their histopathological types (3). Both of these two facts are imposing a diagnostic challenge for salivary tumors. Although Fine-needle aspiration (FNA) has gained wide acceptance as a first-line diagnostic procedure in the diagnosis of salivary gland lesions, and it has variable reported accuracy rates of 74–98%. Now DWI is increasingly used in oncology patients as it reflects data about the cellularity of tissues and thus may suggest the histopathological type preoperatively.

The most common used diffusion method is EPI which is not susceptible to motion artifacts due to rapid acquisition, however it is inherently susceptible to image distortion (5).

DWI in head and neck region is technically demanding due to the presence of multiple bone-air interfaces as well as possibility of involuntary movement of the patient as the act of deglutition (6). Several technical parameters may be achieved due to increase signal-to-noise ratio and spatial resolution for example increasing the acquisition time and application of fat suppression techniques (7).

Even more application of Non-EPI methods such as PROPELLER (Periodically Rotated Overlapping parallel lines with enhanced reconstruction) reduces motion artifacts by means of oversampling of K-space. However, discussion of such technical details is beyond this article. Also fast advanced spin echo [FASE] and split echo acquisition of fast spin echo [SPLICE] reduced the sensitivity to susceptibility artifacts in imaging of head and neck region (8).

Dynamic enhanced MRI has been used in oncological research in different body parts. In salivary gland tumors both quantitative and semi-quantitative methods have been used. In our study, the semi-quantitative one is used which uses

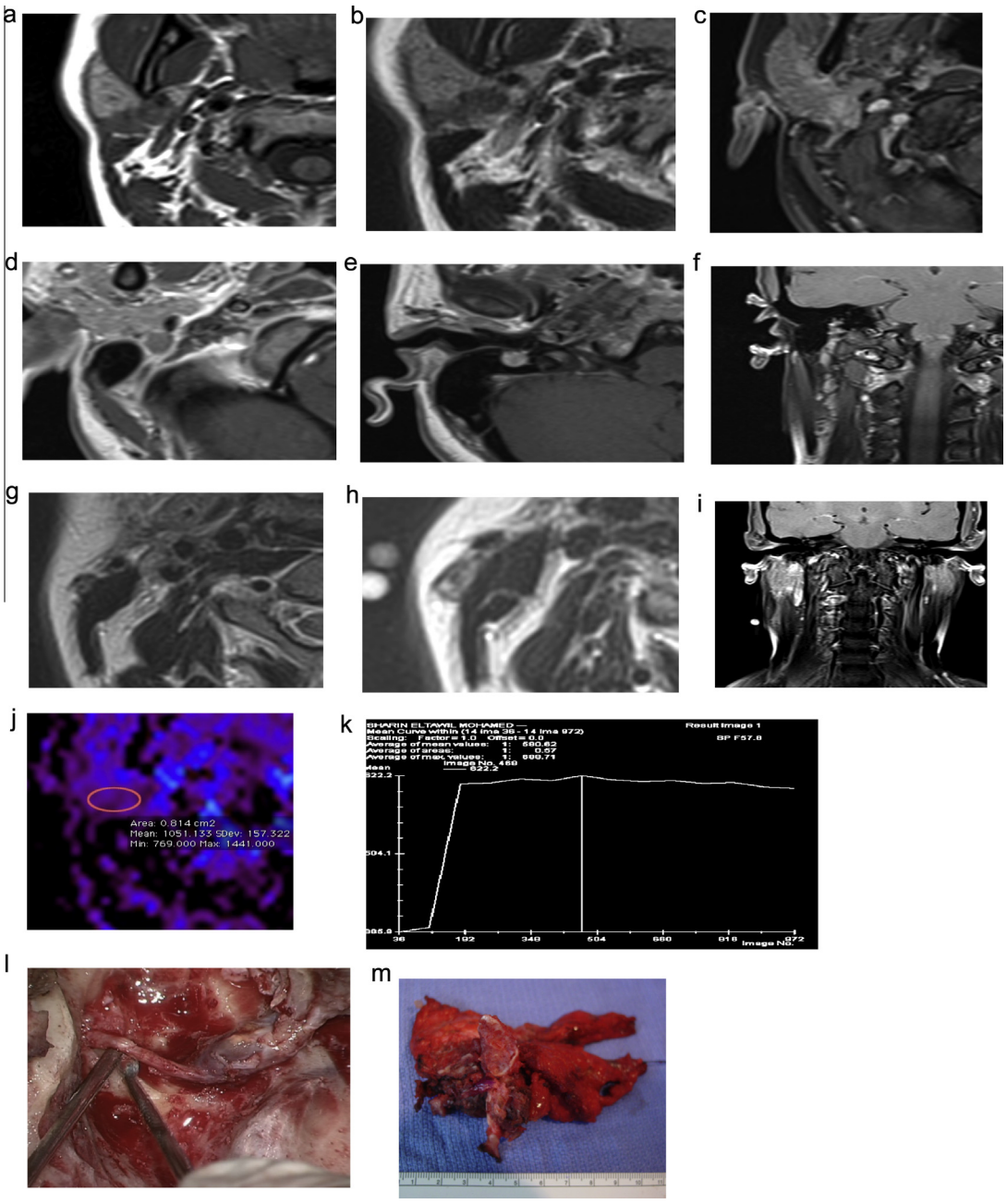

Fig. 8 Case 5: An interesting case report of perineural spread from adenoid cystic carcinoma in young 32 years old female, showing unusual perineural spread along great auricular nerve in addition to spread along facial nerve. (a and b) Axial T1 images in two panes showed lobulated hypo-intense small lesions with ill defined borders and homogenous solid and moderate contrast enhancement of the lesion in post GAD image (c). (d and e) Sequential axial post contrast T1 images revealing abnormal soft tissue thickening and enhancement along the course of intraparotid VII nerve. (g and h) Sequential T2 WI in axial planes showed nodular thickening superficial to the SCM and behind the signal void external jugular vein. This corresponded to perineural spread along the great auricular nerve. Coronal post GAD image in (i) showed enhancing cord like structure. (j) Color scale ADC map revealed intermediate ADC value of 1.01×10^{-3} cm^2/s, with type C of DCE curve revealed in (k). (o and p) Showed surgical specimens with cord like thickening of involved great auricular nerve. *Conclusion* by imaging was made of malignant parotid lesion exhibiting perineural spread along VII and great auricular nerves proven later by surgical biopsy following parotidectomy with sacrifice of VII nerve and dissection of great auricular nerve. Underlying histopathology was of Adenoid cystic carcinoma.

relaxation effect of contrast in tissues and capillaries with drawing of enhancement curves. Semi-quantitative metrics are thus deduced which give indirect data about tissue vascularity and angiogenesis (9).

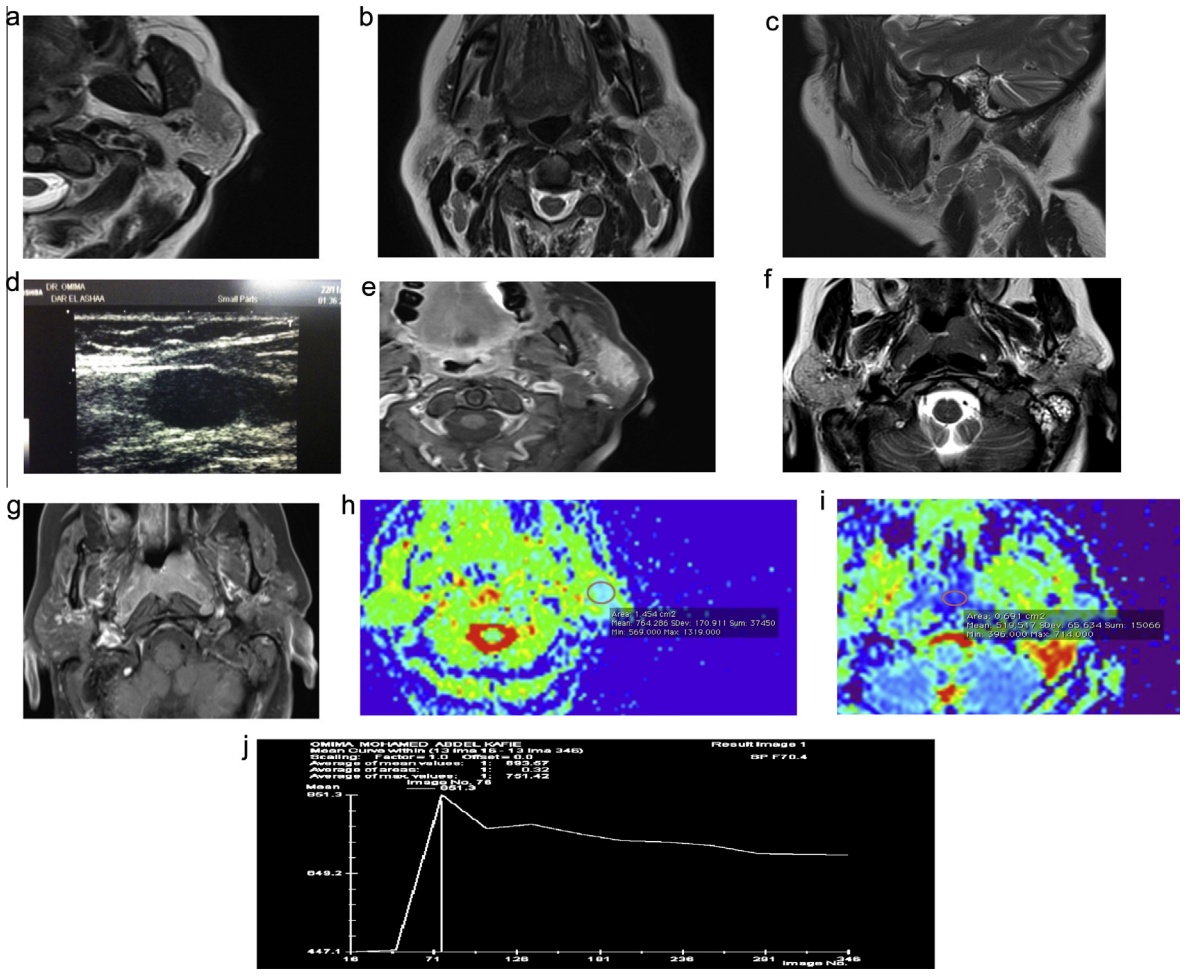

Fig. 9 Case 6: Non-Hodgkin lymphoma. A 60 years old female presented with bilateral cervical neck swellings and left peri-auricular swelling slowly growing over several months. Axial T2 images in (a and b) showed ill defined hypo-intense lesion located in the left parotid in (a) and bilateral deep cervical lymph nodes shown in sagittal T2 image in (c). Ultrasound image of the node (d) revealed marked hypo-echogenicity. Axial post GAD T1 image in (e) showed homogenous solid moderate enhancement of the lesion. Axial T2W in (f) showed asymmetrically prominent nasopharyngeal tissue on left side expanding left fossa of Rosenmüller. This exhibited hypo-intense signal with homogenous moderate post GAD enhancement. (g) Color scale ADC maps showed low ADC value obtained from parotid lesion and cervical nodes (h and i). (j) Revealed high washout ratio suggested by Type-B curve. *Conclusion* was made of Lymphoma of nodal and extra-nodal lymphatic tissues (Nasopharyngeal adenoid and left parotid). Confirmation was later made by nodal Biopsy which revealed non-Hodgkin lymphoma.

In the present study, the diagnostic value of quantitative DW-MRI for parotid gland masses was evaluated in combination with Dynamic enhancement curves.

Representative data on diffusion revealed that pleomorphic tumors had the highest ADC values on DWI ($\geqslant 1.4 \times 10^{-3}$ - cm^2/s), Warthin tumors had low values (0.6–0.8), while malignant tumors had intermediate values (0.8–1.2). This was in accordance with most of research studies (10–12).

First we tried to differentiate between benign and malignant salivary gland lesions with the use of certain cutoff value. We found that a cutoff point for the ADC value at 1.30 and 1.2 could differentiate benign from malignant tumors with 100% sensitivity, 56% specificity, 40% positive and 100% negative predictive values respectively. Comparable results by Inci et al. (13) showed that a cutoff point for the ADC value at 1.30 had 87.50% sensitivity, 58.82% specificity, 50% positive and 96% negative predictive values respectively.

However, ADC values of Warthin tumor overlap with those of malignant parotid tumors in their series. Comparably, Wang et al. (14) reported that mean ADC values of benign solid lesions were significantly higher than those of malignant tumors. In their study, a threshold ADC value of 1.22 provided an accuracy of 86%, sensitivity of 84% and specificity of 91% for predicting malignancy. We concluded that the use of cutoff value was not useful since Warthin tumor and lymphomas have comparable low values.

Secondly we tried to compare tumor groups. We found pleomorphic adenomas to have significantly higher ADC values than Warthin, lymphoma and malignancy. Inci et al. (5) reported that the mean ADC value of the pleomorphic adenomas ($1.8 \times 10^{-3}\,cm^2/s$) was significantly higher than the Warthin tumors which showed average ADC value of $0.8 \times 10^{-3}\,cm^2/s$. Also, the mean ADC value of the pleomorphic adenomas was significantly higher than the malignant

Table 1 Distribution of parotid tumors according to Histopathological diagnosis.

(n = 45)	No.	%
Benign (n = 33)		
BMT	21	63.6
Warthin	11	33.3
Schwanoma	1	3.0
Malignant (n = 12)		
Acinic cell carcinoma	3	25.0
SCC	2	16.7
Muco-epidermoid Carcinoma	2	16.7
Lymphoma	2	16.7
Carcinoma ex-pleomorphic	1	8.3
Adenoid-cystic carcinoma	1	8.3
Parotid metastasis	1	8.3

Table 2 Distribution of ADC level with histopathological.

	Low ADC <0.8 (n = 15)		Intermediate 0.8 to <1.4 (n = 12)		High $\geqslant 1.4$ (n = 21)	
	No.	%	No.	%	No.	%
BMT	0	0.0	0	0.0	21	100.0
Warthin	10	66.7	1	8.3	0	0.0
Malignancy	0	0.0	10	83.3	0	0.0
Lymphoma	2	13.3	0	0.0	0	0.0
BLEL	1	6.7	0	0.0	0	0.0
Lymph nodes	2	13.3	1	8.3	0	0.0

tumors which showed mean ADC of 1.2. Comparably, Blacik et al. (15) reported high ADC values of pleomorphic adenomas to be significantly higher than both Warthin and malignant tumors.

Comparable results by Eida et al. (16) who showed that with the use of extremely high ADCs (typical of pleomorphic adenoma), the difference between benign and malignant lesions was statistically significant.

Table 4 Agreement (sensitivity, specificity and accuracy) for ADC with benign and malignant groups.

ADC	Sensitivity	Specificity	PPV	NPV	Accuracy
1.0	75.0	58.54	34.62	88.89	62.26
1.1	100.0	56.10	40.0	100.0	66.04
1.2	100.0	56.10	40.0	100.0	66.04
1.3	100.0	56.10	40.0	100.0	66.04
1.4	100.0	46.34	35.29	100.0	58.49
1.5	100.0	43.90	34.29	100.0	56.60

However, Warthin Tumors had some confusing results among literature. Group comparison in our study showed that the mean ADC value of the Warthin was significantly lower than the malignant tumors, and "malignant" here excluded Lymphoma.

In disagreement with our results, Habermann et al. (17) reported that ADC values of Warthin tumor ranged from 0.72 to 1.1×10^{-3} cm^2/s, showing an overlap with those of examined malignant lesions (0.79–1.65). Also, Yerli et al. (18) also reported that the mean ADC for malignant tumors was not significantly different from the mean ADC for Warthin tumors. On the other hand, Goyault et al. (19) reported low values of only 0.8 for malignant lesions, while Celebi et al. (20) reported higher values for Warthin reaching 0.9 with consequent overlap between values for Warthin and malignancies.

However, in agreement with our study, Blacik et al. (7) found that Warthin tumors with mean ADC value of 0.9 had significantly lower values than malignant tumors. They found that the use of cutoff value of 1.0×10^{-3} cm^2/s could differentiate malignant lesions from Warthin tumors by sensitivity of 93.2% and specificity of 100%. Also Ikeda et al. (21) reported that the ADC values in Warthin tumors (0.9 ± 0.1) were significantly lower than malignant tumors ($1.10.19 \times 10^{-3}$ cm^2/s). Similar results were concluded by Mootori et al. (22) explaining for Disagreeing results that showed low ADC-values for malignant tumors are likely because these studies included "lymphomas" in malignancies and also included high-grade unusually Hypercellular lesions.

Table 3 Relation between histopathological with ADC.

	BMI (n = 21)	Warthin (n = 11)	Lymphoma (n = 2)	Malignant (n = 10)	$^{KW}\chi^2$	p
ADC						
Min.–Max.	1.40–2.20	0.60–0.90	0.55–0.60	0.80–1.10	37.012*	<0.001*
Mean ± SD	1.79 ± 0.27	0.69 ± 0.08	0.58 ± 0.04	0.97 ± 0.10		
Median	1.80	0.70	0.58	0.98		
Sig. bet. Grps.	$p_1 < 0.001$*, $p_2 = 0.021$*, $p_3 < 0.001$*, $p_4 = 0.038$*, $p_5 < 0.001$*, $p_6 = 0.030$*					

$^{KW}\chi^2$: Chi square for Kruskal Wallis test.
Sig. bet. grps using Mann Whitney test.
p_1: p value for comparing between BMI and Warthin.
p_2: p value for comparing between BMI and Lymphoma.
p_3: p value for comparing between BMI and Malignant.
p_4: p value for comparing between Warthin and Lymphoma.
p_4: p value for comparing between Warthin and malignant.
p_4: p value for comparing between lymphoma and malignant.
* Statistically significant at $p \leqslant 0.05$.

Table 5 Agreement (sensitivity, specificity and accuracy) for ADC with benign and malignant groups.

ADC	Benign (n = 41)	Malignant (n = 12)	Sensitivity	Specificity	PPV	NPV	Accuracy
⩾1.4	23	0	100.0	56.10	40.0	100.0	66.04
<1.4	18	12					
Other	38	2	83.33	92.68	76.92	95.0	90.57
0.8 to <1.4	3	10					

Table 6 Distribution of type of DCE among histopathological diagnoses.

Histopathological	Type DCE			
	A	B	C	D
Benign				
BMT	19	0	2	0
Warthin	0	11	0	0
Lymph nodes	0	3	1	0
BLEL	0	1	0	0
Chronic inflammatory	0	0	2	0
Cyst	0	0	0	1
Schwanoma	1	0	0	0
Malignant				
Acinic cell carcinoma	0	1	2	0
SCC	0	0	2	0
Adenoid cystic carcinoma	0	0	1	0
Lymphoma	0	2	0	0
Carcinoma ex-pleomorphic	0	0	1	0
Mucoepidermoid	1	0	1	0

Although in our study Warthin had significantly higher values than lymphoma, this difference is of little help in clinical practice since both have overlapping ADC-values. Histological nature of both lesions, both rich in lymphocytes explains low ADC values. We concluded that DWI is not helpful to differentiate lymphoma from Warthin, and morphological criteria can be more helpful.

Thirdly we tried to use certain ADC values and ranges to separate pathological groups. Statistical analysis in our study pointed out that using a high ADC value ⩾1.4 as a sign of benignity showed a moderate accuracy of 66%, while using intermediate ADC (in range of 0.8 to <1.4) appeared to be a useful test of malignancy showed a high accuracy of 90%.

In agreement with our results, Yerli et al. (23) made a comparative study between MRI-DWI and adequate FNAC regarding accuracy in diagnosis of salivary glandular tumors. They used ADC values greater than 1.3 to be suggestive of pleomorphic adenoma, masses with ADC values lower than 1.1 as Warthin tumors, and values (1.1–1.3) as malignant tumors. They found that "adequate" FNAC and MRI-DWI had comparable accuracy in differentiating parotid lesions.

Regarding dynamic curves we followed those used by Yabuuchi et al. (3). They analyzed four TIC parameters regarding two parameters: the T-peak and Washout ratios (WR). According to their results, T-peak correlated closely with microvessel count and the Washout ratio (WR) accurately reflected the cellularity-stromal grade. Comparable to Yabucchi et al. (3), our series revealed that Type A curve predominated the pleomorphic adenomas-apart from single case of carcinoma-ex-pleomorphic-, type B curve predominated Warthins, and other lymphoid lesions as lymphoma and benign lymph nodes since compact lymphocytes in these lesions account for high (WR). Finally Type C curve predominated malignant lesions except two cases of pleomorphic adenomas.

Statistical analysis in our series showed that Type A curve as a test of benignity showed accuracy of only 58.8%, while type C curve appeared to be a useful test of malignancy show-

Table 7 Agreement (sensitivity, specificity and accuracy) for DCE with benign and malignant groups.

DCE	Benign (n = 41)	Malignant (n = 11)	Sensitivity	Specificity	PPV	NPV	Accuracy
A	20	1	90.91	50.0	33.33	95.24	58.82
B + C	20	10					
A + B	35	4	63.64	87.50	58.33	89.74	82.35
C	5	7					

Table 8 Agreement (sensitivity, specificity and accuracy) for combined ADC + DCE with benign and malignant groups.

Combined ADC + DCE	Benign (n = 41)	Malignant (n = 11)	Sensitivity	Specificity	PPV	NPV	Accuracy
A + high	20	0	100.0	48.78	34.36	100.0	59.62
Other	21	11					
Other	40	4	63.64	97.56	87.50	90.91	90.38
C + intermediate	1	7					

ing moderate 63% sensitivity and high specificity of 87.5%, and good accuracy of 82.3%.

Suengo et al. (24), Hazem et al. (25) and Hisatomi et al. (26) studied dynamic curves with quantitative parameters parallel to those analyzed by Yabucchi and found that these curves could successfully differentiate salivary gland tumors.

Yabuuchi et al. (3) later analyzed the curve in combination with diffusion and made a diagnostic algorithm that made the basis for our study.

A comparable work combining DWI and DCE was made by Eida et al. (27). They defined four TIC patterns (1–4) comparable to those of Yabbuuchi in combination with four values of ADC in calculated tumoral areas by the use of sophisticated software. They had the following conclusions:

- In disagreement with Yabuuchi who considered type A curve only a benign curve, Eida et al. (18) found few malignant lesions to exhibit this curve. This was in accordance with our study, which revealed type A curve in a single malignant case of carcinoma ex-pleomorphic who also had low ADC value.
- Again Eida et al. (18) found lesions with (type C curve) were all malignant. This is contradictory to those by Yabuuchi and ours since this curve was exhibited by pleomorphic adenoma.
- Finally in agreement with our study, Eida et al. (18) reported that salivary gland tumors with Type 4 curve (type B curve) predominated Warthin's tumors and lymphomas.

Finally in our study we attempted to test the combination of Type A curve and High ADC value $\geqslant 1.4 \times 10^{-3}$ cm^2/s as a test of benignity which yielded accuracy of only 59.6%. On the other hand, a combination of Type C curve and Intermediate ADC values $(0.8–1.4) \times 10^{-3}$ cm^2/s was tested a test of malignancy and showed a high accuracy of 90%.

The main limitation in our study was the limited number of tumors due to relative rarity of salivary tumors. Also the role of FNAC has not been addressed, and this is because FNA results were not always available before MR imaging.

In conclusion, MRI with the use of novel sequences including diffusion and enhancement curves is a valuable tool in preoperative work-up of salivary tumors including differentiation of histopathology, which can be an adjunct to FNAC. Combined interpretation of DWI and DCE curves is more helpful than use of single technique. Combination of intermediate ADC values and Type C curve can suggest malignant lesion.

Conflict of interest

The authors declare that there are no conflicts of interest.

References

(1) Som PM, Brandwein M. Salivary glands. In: Som PM, Curtin HD, editors. Head and neck imaging. 3rd ed., vol. 2. St. Louis, MO: Mosby-Year Book, Inc.; 1996. p. 877–912.
(2) Thoeny Harriet C. Imaging of salivary gland tumours. J Cancer Imaging 2007(7):52–62.
(3) Arrangoiz R, Papavasiliuo P, Sarcu D, Galloway TJ, Ridge JA, Lango M. Current thinking on malignant salivary gland neoplasms. J Cancer Treat Res 2013;1(1):8–24.
(4) Yabuuchi H, Matsuo Y, Kamitani T, Setoguchi T, Okafuji T, Soeda H, et al. Parotid gland tumors: can addition of diffusion-weighted MR imaging to dynamic contrast-enhanced MR imaging improve diagnostic accuracy in characterization? Radiology 2008;249:909–16.
(5) Turkbey B, Aras O, Karabulut N, Turgut A, Akpinar E, Alibek S, et al. Diffusion weighed MRI imaging in detecting and monitoring cancer: review of current applications in body imaging. Diagn Interv Radiol 2012;18:46–59.
(6) Chikui T, Ohga M, Kitamoto E, Shiraishi T, Kowano S, Yoshura T, et al. Quantification of diffusion and permeability of MRI in head and neck region. J Radiol Radiat Ther 2014(2):1047.
(7) Barbero J, Jimenez I, Noguerol T, Alcala A. Utility of MRI diffusion techniques in the evaluation of head and neck tumors. Cancers 2013(5):875–89.
(8) Serifoğlu I, Ilker Oz I, Damar M, Tokgöz Ö, Yazgan Ö, Erdem Z. Diffusion-weighted imaging in the head and neck region: usefulness of apparent diffusion coefficient values for characterization of lesions. Diagn Interv Radiol 2015;21:208–14.
(9) Gordon Y, Partovi S, Müller-Eschner M, Amarteifio E, Bäuerle T, Weber MA, et al. Dynamic contrast-enhanced magnetic resonance imaging: fundamentals and application to the evaluation of the peripheral perfusion. Cardiovasc Diagn Ther 2014;4(2):147–64.
(10) Matsushima N, Maeda M, Takamura M, Takeda K. Apparent diffusion coefficients of benign and malignant salivary gland tumors. Comparison to histopathological findings. J Neuroradiol 2007;34(3):183–9.
(11) Nagata S, Nishimura H, Uchida M, Sakoda J, Tonan T, Hiraoka K, et al. Diffusion-weighted imaging of soft tissue tumors: usefulness of the apparent diffusion coefficient for differential diagnosis. Radiat Med 2008;26(5):287–95.
(12) Maeda M, Marien S. Usefulness of diffusion-weighted imaging and apparent diffusion coefficients in the assessment of head and neck tumors. J Neuroradiol 2008;35:71–8.
(13) Inci E, Hocaoğlu E, Kiliçkesmez Ö, Aydin S, Cimilli T. Quantitative diffusion-weighted MR imaging in the differential diagnosis of parotid gland tumors: is it a useful technique? Turk J Med Sci 2010;30(4):1339–45.
(14) Wang J, Takashima S, Takayama F, et al. Head and neck lesions: characterization with diffusion-weighted echo-planar MR imaging. Radiology 2001;220(3):621–30.
(15) Blacik C, Akan H, Inceso. Evaluating parotid tumors according to diffusion weighed MRI. Eur J Gen Med 2014;11(2):77–84.
(16) Eida S, Sumi M, Sakihama N, Takahashi H, Nakamura T. Apparent diffusion coefficient mapping of salivary gland tumors: prediction of the benignancy and malignancy. AJNR Am J Neuroradiol 2007;28:116–21.
(17) Habermann CR, Arndt C, Graessner J, Diestel L, Petersen KU, Reitmeier F, et al. Diffusion-weighted echo-planar MR imaging of primary parotid gland tumors: is a prediction of different histologic subtypes possible? J Neuroradiol 2009;30:591–6.
(18) Yerli H, Agildere AM, Aydin E, Geyik E, Haberal N, Kaskati T, et al. Value of apparent diffusion coefficient calculation in the differential diagnosis of parotid gland tumors. Acta Radiol 2007;48(9):980–7.
(19) Goyault L, Riehme S, Neuville A, Gentine A, Veillon A. Interest of diffusion weighed and gadolinium enhanced dynamic MR sequences for diagnosis of parotid gland tumors. J Neuroradiol 2011;38:77–89.
(20) Celebia I, Mahmutoglua AS, Ucgula A, Ulusaya AM, Basakb T, Basaka M. Quantitative diffusion-weighted magnetic resonance imaging in the evaluation of parotid gland masses: a study with histopathological correlation. Clin Imaging 2012;4(25):1–7.
(21) Ikeda M, Motoori K, Hanazawa T, Nagai Y, Yamamoto S, Ueda T, et al. Warthin tumor of the parotid gland: diagnostic value of MR imaging with histopathologic correlation. AJNR Am J Neuroradiol 2004;25:1256–62.

(22) Motoori K, Yamamoto S, Ueda T, Nakano K, Muto T, Nagai Y, et al. Inter- and intratumoral variability in magnetic resonance imaging of pleomorphic adenoma: an attempt to interpret the variable magnetic resonance findings. J Comput Assist Tomogr 2004;28:233–46.
(23) Yerli H, Aydin E, Haberal N, Harman A, Kaskati T, Alibek S. Diagnosing common parotid tumours with magnetic resonance imaging including diffusion-weighted imaging vs fine-needle aspiration cytology: a comparative study. Dentomaxillofacial Radiol 2010;39:349–55.
(24) Suenaga S, Indo H, Noikura T. Diagnostic value of dynamic magnetic resonance imaging for salivary gland diseases: a preliminary study. Dentomaxillofacial Radiol 2001;30:314–8.
(25) El Shahat H, Fahmy HS, Gouhar GH. Diagnostic value of gadolinium-enhanced dynamic MR imaging for parotid gland tumors. Egypt J Radiol Nucl Med 2013;44:203–7.
(26) Hisatomi M, Saumi JI, Yanagi Y, Unetsubo Y, Maki Y, Murakami J. Diagnostic value of dynamic contrast-enhanced MRI in the salivary gland tumors. J Oral Oncol 2006;43(9):940–7.
(27) Eida S, Sumi M, Nakamura T. Multiparametric magnetic resonance imaging for the differentiation between benign and malignant salivary gland tumors. J Magn Reson Imaging 2010;31:673–9.